
Article:
Wang, J.-Y., Mullin, N. and Hobbs, J.K. (2018) High-speed large area atomic force microscopy using a quartz resonator. Nanotechnology, 29 (33). 335502. ISSN: 0957-4484

https://doi.org/10.1088/1361-6528/aac7a3

High-speed large area atomic force microscopy using a quartz resonator

J-Y Wang[1], N Mullin[1], and J K Hobbs[1]
[1]Department of Physics and Astronomy, Hicks Building, University of Sheffield, S3 7RH

E-mail: jamie.hobbs@sheffield.ac.uk

Abstract
A high-speed atomic force microscope for scanning large areas, utilising a quartz bar driven close to resonance to provide the motion in the fast scan axis is presented. Images up to 170 x 170 μm^2 have been obtained on a polydimethylsiloxane (PDMS) grating in 1 second. This is provided through an average tip-sample velocity of 28 cm/sec at a line rate of 830 Hz. Scan areas up to 80 x 80 μm^2 have been obtained in 0.42 seconds with a line rate of 1410 Hz. To demonstrate the capability of the scanner the spherulitic crystallization of a semicrystalline polymer was imaged *in situ* at high speed.

1. Introduction

High-speed atomic force microscopy (HS-AFM) was first introduced by Barrett *et al* in the early 1990s for imaging metal-semiconductor films [1]. The scan rate has been increased by 2-3 orders of magnitude compared to conventional AFM and achieved an imaging rate of several frames per second with scan sizes from a few hundred nanometers to tens of microns. To image at high speed without compromising spatial resolution, numerous efforts have been put into developing robust mechanical scanners along with high-bandwidth feedback control systems [2-9], small cantilevers with high resonance frequencies [10-14], sensitive optical detection systems with sufficiently small laser spot sizes to detect them [15-17] and fast data acquisition systems [18]. The increasing scan rate has enabled the study of dynamic processes at sub-second timescales [17, 19-24] and has increased the throughput of AFM to a level where it is a viable technique for use in applications such as semiconductor process control [25].

To maintain controlled scanner motion at high scan rates, the design and control of mechanical scanners has played a crucial role in the development of HS-AFM systems [26, 27]. Small, stiff scanners based on piezo tubes [2,3] or flexures optimized using finite element methods [4,6,18,28,29-31] allow control to be maintained at high frequencies, but often at the expense of maximum scan size [32-34]. Notch filtering and model based feedback have allowed scanners to be driven at higher frequencies while mitigating the effects of resonant behavior [26,27,35,38,39], and non-raster scanning techniques such as Lissajous [40] and spiral scanning [41-43] allow control at high scan rates as the scanner drive signals do not contain components at higher harmonics of the scan frequency.

An alternative approach which we have previously employed [44] is to use the mechanical resonance of the scanner itself to provide the fast scan axis, an approach termed resonant scanning. In resonant scanners the scanner is driven sinusoidally at its resonant frequency, leading to a sinusoidal tip-sample displacement and greatly increased amplitude due to the action of resonance. This resonant amplification and well-described trajectory allow relatively straightforward construction of large area, high-speed scanners as the generation of complex drive waveforms at high voltage and their accurate transduction into linear physical displacements is not required [44-52]. The non-linear displacement is typically corrected by mapping the data directly onto position using the known sinusoidal relationship between displacement and time for a harmonic oscillator [45]. A wide-area scanner was developed in previous work using a macroscopic quartz bar resonator as the fast scanner [44]. A scan area of 37.5 x 37.5 μm^2 was obtained in 0.7 seconds with a line rate of 772 Hz in

quasi-constant height contact mode.

In this work, a resonant scanner was constructed using a similar macroscopic quartz bar resonator as previously [44] but with modified dimensions and drive mechanism to give considerably improved performance. A substantially larger area of 170 x 170 μm^2 could be scanned in 1 second with an average tip-sample velocity of 28 cm/sec. This is significantly beyond the scan areas that have been obtained using more conventional scanning approaches and shows the utility of resonance when exploring the extremes of scanner performance. The new scanner was tested on gratings made from polydimethylsiloxane (PDMS), and by following the crystallization of a semi-crystalline polymer *in situ*.

2. Experimental Methods

2.1 Scanner design

The high speed large area AFM scanner ideally needs to maintain planar motion over the full scan area while also allowing the maximum possible scan area. As in our previous work, a quartz bar was selected for the resonant scanner because of the high rigidity, low mechanical losses and thermal stability of quartz. A number of different geometries of the resonator were tested using a finite element model (FEM) developed in COMSOL MULTIPHYSICS (Ver 5.1), from iterations of the previous design [44] to geometries where both ends of the bar were clamped and the central region driven into resonance. The final design is shown in figure 1(a) and provided the best combination of high amplitude and planar scanning. One end of the quartz bar is fixed in a steel holder and a drive piezo (PL055, PICMA Chip Actuator, Physik Instrumente Ltd., Germany) is positioned in contact with the side of the bar at a distance of approximately one sixth of the beam length from the fixed end. The sample is mounted on the top surface of the bar, close to the free end. As described in our previous work [44], the resonant frequency of the bar may be varied by adjusting the fixing point (and hence the effective length of the bar) in the steel holder. Beam theory predicts that reducing the length will cause the resonant frequency (and hence scan rate) to increase in proportion to the inverse square of the free length [53].We have verified this for our scanner using FEM simulation, the results of which are plotted in figure 1(b). The drive mechanism differs from the previous design [44] in the positioning of the drive piezo against the bar away from the fixed end (as opposed to clamping the bar and piezo together at the fixed end, in the previous design), which allows significantly larger amplitudes (and hence scan sizes) to be obtained as the piezo motion is no longer constrained by the steel holder. The quartz bar used in this work was thicker and less tall (4 mm x 5.5 mm x 66 mm (thickness x height x length)) than the previous design (2 mm x 10 mm x 65 mm) to increase resonant frequency and thus imaging rate.

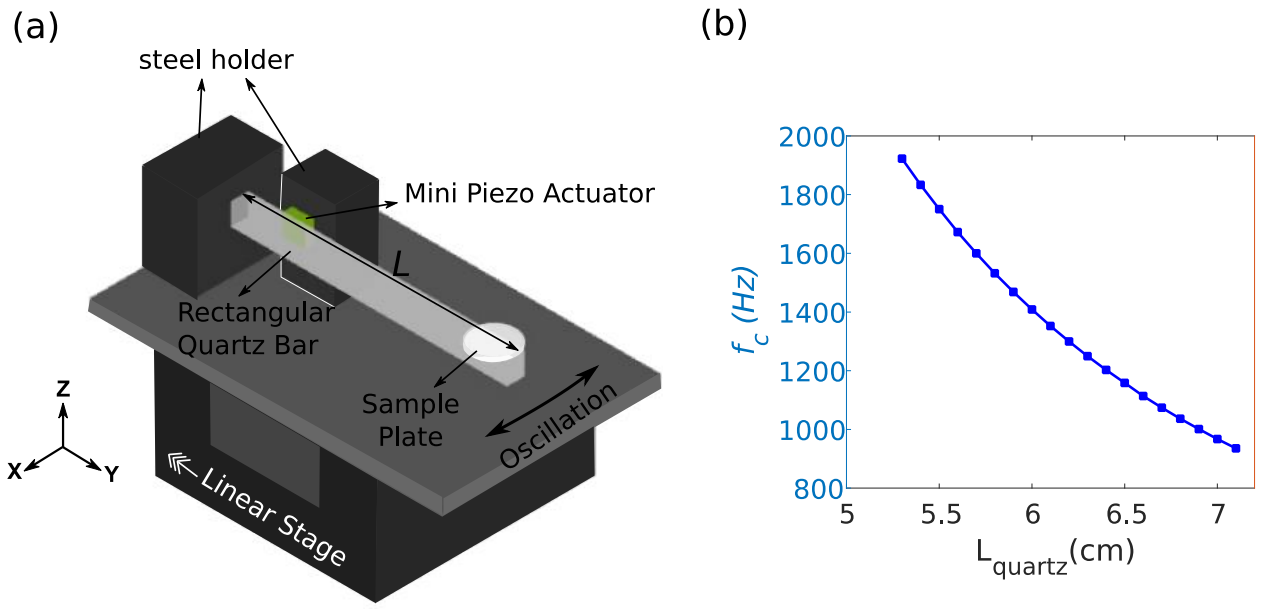

Figure 1 A schematic diagram of the quartz bar resonant scanner. One end of the quartz bar is fixed to the holder either with glue or by clamping with a screw. A piezo actuator is brought into contact with the quartz bar and drives the oscillation along the X direction. The sample is placed at the free end of the quartz bar. A linear nano-positioning stage is placed underneath the holder to provide the slow scan axis along the Y direction. (b) The resonant frequency (f_c) of the quartz bar (calculated from FEM simulation) plotted against length L.

When developing a scanner for high speed motion over large areas one of the potential issues is development of unwanted vertical motion of the scanning stage. This can lead to image distortion or, in the case of constant-height scanning, very high tip-sample forces. FEM has been used to simulate the displacement of the quartz bar in the lateral (X) and vertical (Z) directions when driven at its first resonant frequency. The results are shown in figure 2. In figure 2(a) and (b), the colour scales represent the displacements of the quartz bar along the X- and Z-axis, respectively. In figure 2(c), a 2D figure of the displacement along the Z-axis is plotted at the site of the sample plate where the arrow marks the centre. However, the FEM program assumes that the piezo actuator is bonded to the quartz bar while in the experimental case these are only pushed into contact with each other, without glue or any other mechanical linkage. Hence the real vertical displacement (and any image distortion that this would be expected to produce) is expected to be smaller than the simulated value due to less direct distortion and coupling from the piezo actuator and the holder.

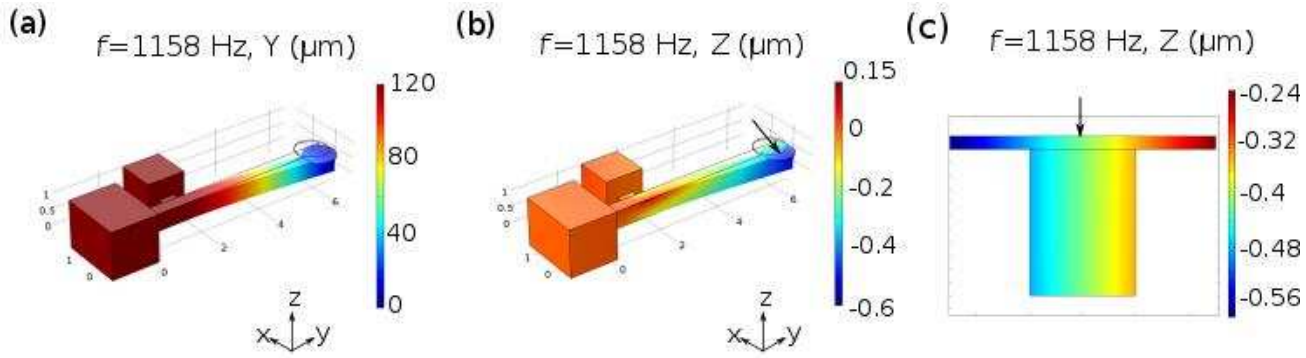

Figure 2 3D FEM simulation of the quartz bar displacement at its first flexural resonance in both (a) lateral (X) and (b) vertical (Z) orientation. (c) is the 2D FEM simulation of the vertical displacement (Z) at the site of sample plate with quartz bar underneath, marked with an arrow in (b).

2.2 System Setup

The quartz bar resonant scanner is placed in the sample space of a tip-scanned AFM (Veeco Dimension 3100, with Nanoscope IV controller), allowing conventional images to be taken of the same area to provide a comparison. The quartz bar holder is placed on a nano-positioning stage (PI611.10 Physik Instrumente Ltd., Germany) which provides the slow scan axis. Both fast and slow scan axes are driven by sinusoidal signals supplied by a VideoAFM controller (Infinitesima Ltd., UK) through two identical amplifier modules (E505.00 Physik Instrumente Ltd., Germany) [45,46]. A 10 mm diameter glass coverslip was placed on top of the free end of the sample scanner, held with a thin layer of rubber adhesive (Reprorubber, Flexbar Corp., US).

During resonant scanning, the AFM is operated in contact mode. The feedback loop of the conventional AFM remains active, but does not respond quickly enough to track the surface at the rate pixels are acquired. As such, the feedback loop only acts to counteract large, slowly varying features on the surface, such as sample slope. A combination of the vertically applied force due to cantilever bending and the attractive force due to the capillary neck keeps the tip in contact with the sample during scanning, providing "passive feedback" [46]. The high speed image is constructed from the vertical deflection signal, accessed from the In0 channel of the Signal Access Module. This is fed into the VideoAFM controller, which samples deflection and corrects for the sinusoidal motion in both the slow and fast scan axes using the known sinusoidal trajectory of the scanner to map the data onto linearly spaced pixels. This is done by the VideoAFM controller in real time using a proprietary routine executed on a field-programmable gate array, in which the phase of the scanner is a free parameter which is adjusted by the user. The resonant frequency of the quartz bar scanner was located by sweeping the drive frequency through a range of 500-2000 Hz while the cantilever was engaged on the sample surface but not scanning. Using this approach, the resonant frequency could be located by monitoring the deflection signal during the sweep. For the data shown here, two different clamping positions were used, with corresponding resonant frequencies of 830 and 1410 Hz. Drive amplitudes up to 160 $V_{p\text{-}p}$ were used. The scan rate (frames/second) along the slow scan axis was set to 0.5 – 1.2 Hz. Only either the up or down scan was collected, in order to avoid image "breathing" due to hysteresis in the slow scan axis. Small, relatively soft cantilevers (Bio-lever Mini BL-AC40TS, Olympus, Japan) with a nominal spring constant k= 0.09 N/m and f=125 kHz were used in this work.

2.3 Sample Preparation

To test the scan size that may be obtained with our scanner, a replica of a 10 μm pitch calibration grating (VGRP-15M, Bruker) was cast using polydimethylsiloxane (PDMS). The original grating consists of square

pits with a period of 10 μm and a depth of 180 nm. The PDMS base and cross-linking agent (Sylgard 184, Dow Corning) were mixed with a mass ratio of 10:1, as recommended by the manufacturer. The mixed PDMS was poured onto the original grating and cured in an oven at 80 ºC for 3 hours followed by 24 hours at room temperature. After curing, the PDMS layer was peeled off the silicon wafer to give a negative replica of the original grating, with square pillars projecting above a planar surface. Imaging with conventional AFM (figure 3) showed that these pillars have a height of approximately 130 nm. This implies some vertical shrinkage during the curing process, but the lateral dimensions remained constant.

To demonstrate the capability of imaging dynamic processes at high speed, crystallization of a polyhydroxybutyrate (PHB) polymer sample was imaged *in situ*. The sample was melted at 200 °C on a glass cover-slip for one to two minutes until it appeared clear. Then the polymer was thinned with a razor blade and quenched to room temperature. It was then glued to the quartz bar and scanned in ambient air. The crystallization started within one to five minutes after being placed at room temperature.

3. Results and Discussion

A contact-mode height image of the PDMS replica, taken using conventional AFM, is shown in figure 3. The image is 80 x 80 μm^2 with 256 x 256 pixels at a line rate of 1 Hz. A height profile taken along the line indicated shows the height of the pillars is approximately 130 nm. High-speed images of the PDMS replicas taken in ambient air with four different scan sizes (from 80 x 80 μm^2 to 170 x 170 μm^2) are shown in figure 4. Each image was captured in one second at a line rate of 830 Hz which corresponds to average sample velocities of 13 – 28 cm/sec (or peak tip-sample velocities 20 - 44 cm/sec). The scan size along the fast scan axis could be increased to as much as 200 μm, while the slow scan axis is limited to a linear range of 170 μm by the stage used. Stability has been tested by running the scanner for extended periods on PDMS gratings. Figure S1 shows individual frames from the same dataset as figure 4. Images were captured for 20 minutes while varying the scan size by adjusting the drive amplitude.

In figure 5(a) and (b) high-speed images from the same PDMS replica gratings were captured at a higher imaging rate by reducing the unclamped length of the quartz bar to 52 mm to increase the resonant frequency (and hence the line rate) to 1410 Hz. This allowed images of 70 x 70 μm^2 and 80 x 80 μm^2 to be captured in 0.42 seconds. From the images presented it is clear that the use of resonance to provide the fast scan axis enables very large area high speed scanning. However, the approach clearly has some disadvantages. Along the fast scan axis, we measure systematic increase in measured feature size from left to right with a maximum error of 11 %, either caused by a mismatch between the actual phase of the resonating scanner and that of the image acquisition and presentation software, or by a departure from simple harmonic motion of the scanner (as this is assumed in the data presentation algorithm) [45,48]. A similar trend is observed along the slow scan axis, with deviations up to 12%, most likely due to nonlinearity in the slow scan stage. As in previous studies where we have used quasi-constant height imaging approach, the image data is not always simple to interpret, with images being more similar to conventional error mode (e.g. “deflection”) than true topographic data [49]. However, this has the advantage that high frequency, low amplitude features, such as small bumps and holes in the PDMS surface, are visible in the high speed images, showing that there are not significant distortions caused by the scanner. High speed scanning requires high tip-sample velocities, and here the large areas are obtained by pushing this parameter higher than in our previous work [44], to a peak value of 44 cm/s (or 28 cm/s average velocity). Considering the relatively challenging topography of the grid sample, it is not surprising that some image degradation is seen at step edges with this large imaging speed, as pixels are being captured at a higher frequency than the cantilever can respond. This leads to “smearing” of the features along the fast scan axis and it may be that the energy dissipating nature of the rubber surface is helpful in maintaining a stable image at the largest scan areas. However, it is likely that tip-sample forces remain high especially when the tip encounters a large vertical step, so we investigated the capability of the scanner for imaging a sample where damaging tip-sample interactions are both easily observable and relatively difficult to

avoid.

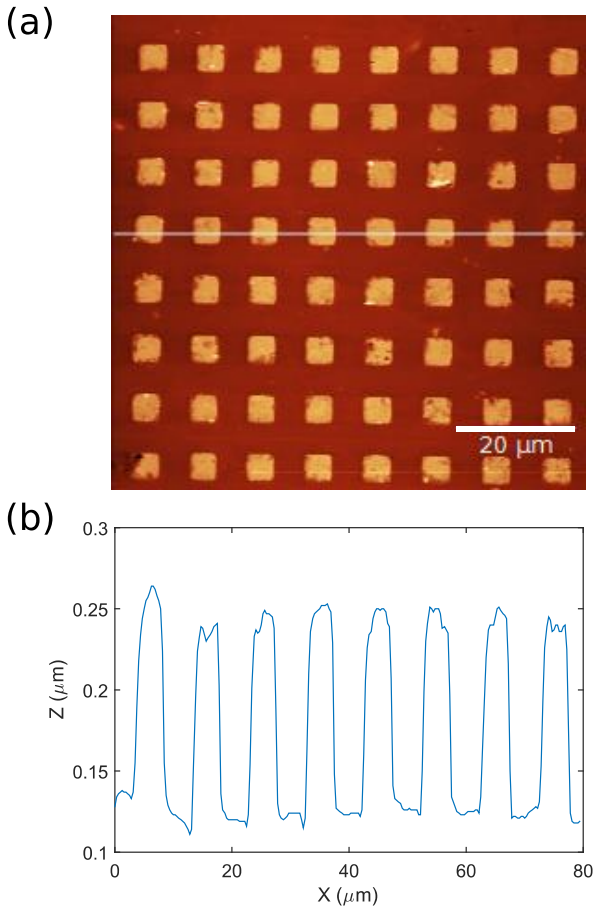

Figure 3 Height image (a) using a conventional contact mode AFM on a PDMS replica of a 10 µm calibration grating. Black to white colour represents 0 to 1.1 µm in (a). Height profile (b) is taken along the marked horizontal line showing square pillars approximately 130 nm high.

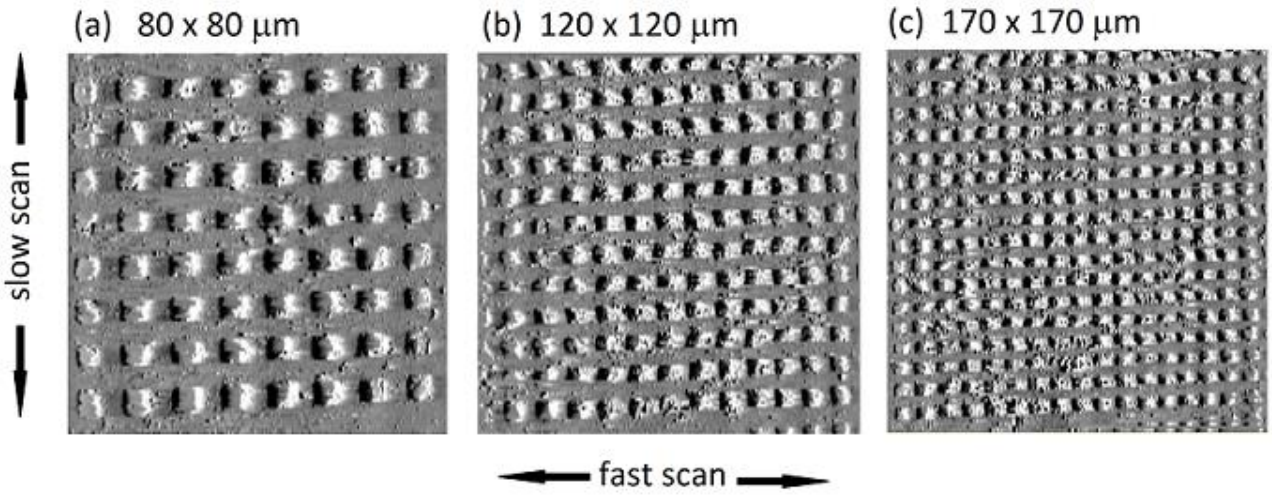

Figure 4 High-speed images on PDMS calibration grid negative replicas, acquired in 1 second. Scan areas from 80 x 80 µm^2 to 170 x 170 µm^2 were obtained by changing the drive amplitude from 41 to 133 $V_{p\text{-}p}$. The

slow scan range is limited to 170 µm. The grey scale represents the deflection signal in arbitrary units.

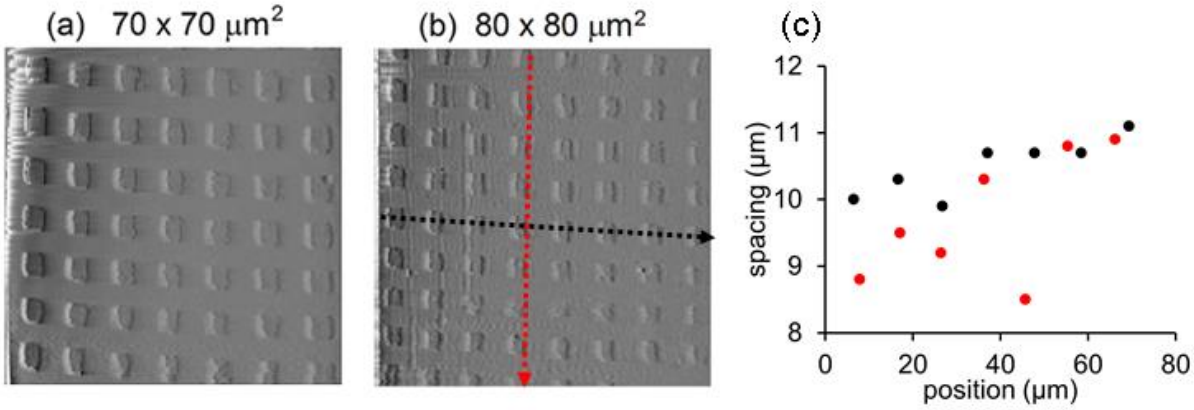

Figure 5 High-speed images on PDMS replicas. By reducing the free length of the quartz bar to increase the resonant frequency to 1410 Hz, image areas of (a) 70 x 70 µm^2 and (b) 80 x 80 µm^2 were captured in 0.42 seconds. The grey scale represents the deflection signal in arbitrary units. (c) Feature spacings measured along the marked lines in (b).

In figure 6 (high-speed movie supplied in SI, 20× true speed), a series of high-speed images are shown from the crystallization process of polyhydroxybutyrate (PHB) polymer at room temperature. The polymer provides a good test for the scanner as both a dynamic process and because the molten polymer (the smooth background in these images) is relatively soft. The crystallization of this polymer is too fast for conventional AFM imaging at room temperature without considerable distortion of spherulite shape caused by the progression of the crystallization process between consecutive scans, whereas in these high speed images the spherulites (disk shaped when grown in approximately 2-D films) appear approximately circular as expected. The scan size is 57 x 62 µm^2. Each image was acquired in 1 second with a line rate of 830 Hz which corresponds to an average tip-sample velocity of 10.8 cm/sec. The image resolution is 256 x 256 pixels (i.e. pixels are slightly asymmetric as the image was collected slightly off-square). A conventional contact mode height image was also collected after crystallization had completed and is shown in figure 7. The smaller frame marked on figure 7 (white dashed rectangle) is the area imaged by the high-speed AFM in figure 6. In the high-speed images of the crystallized surface (figure 6), imaging artifacts appeared at the junctions between spherulites due to the AFM tip failing to track the sample surface at steep features. The height profiles from three horizontal lines (1-3) from the conventional AFM image are plotted in figure 7b.

Comparison between the high-speed image and the conventional AFM image shows that there is good agreement between the two approaches, with fine features being identifiable across the two sets of data. From the accompanying movie (SI2) the right hand spherulite appears oval in the initial images before adopting the expected circular shape. This is most likely because of the unusual growth mode of PHB spherulites at a surface which leads to the rapid growth rates observed here [54]. If tip-sample forces, and in particular shear forces, were high we would expect the AFM tip to induce nucleation in the amorphous polymer regions, leading to crystallization happening outside of the circular radiating domains, and this is not seen. Indeed, in previous studies we have found that if imaging in contact mode with conventional AFM on small scan areas (i.e. a few micrometres or less) very rapid crystal nucleation is induced [55]. We therefore conclude that, on the relatively flat molten areas, imaging forces are not substantially higher than in conventional contact mode AFM imaging, or that at least the impact of higher forces is mitigated by the visco-elastic response of the polymer.

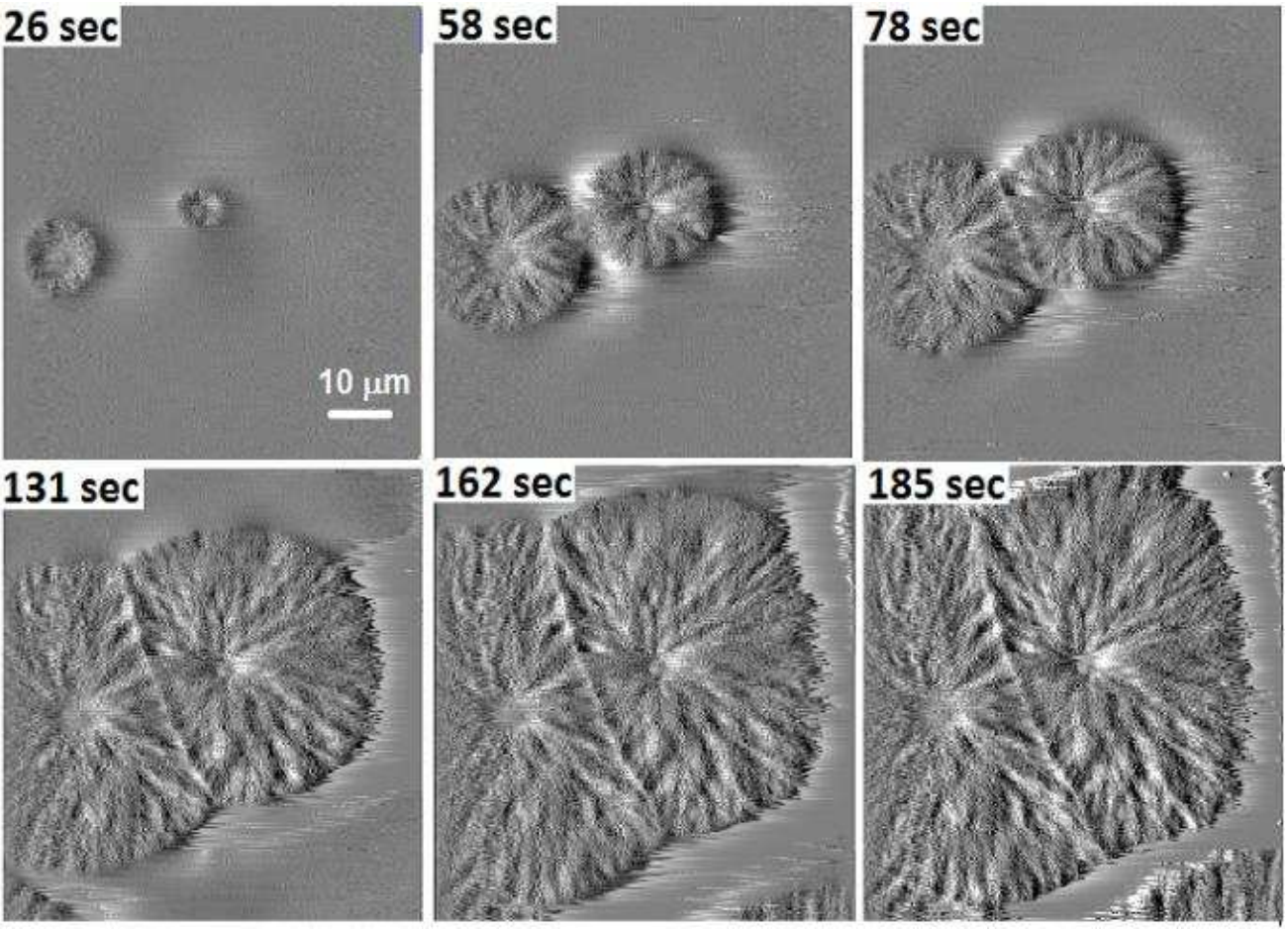

Figure 6 A series of the high-speed AFM images from the crystallization process of polyhydroxybutyrate (PHB) polymer at room temperature where the growth of two spherulites was captured on the surface. Images were acquired in one second each with a line rate of 830 Hz. The image size is 57 x 62 μm^2 and the image resolution is 256 x 256 pixels. The grey scale represents the deflection signal in arbitrary units.

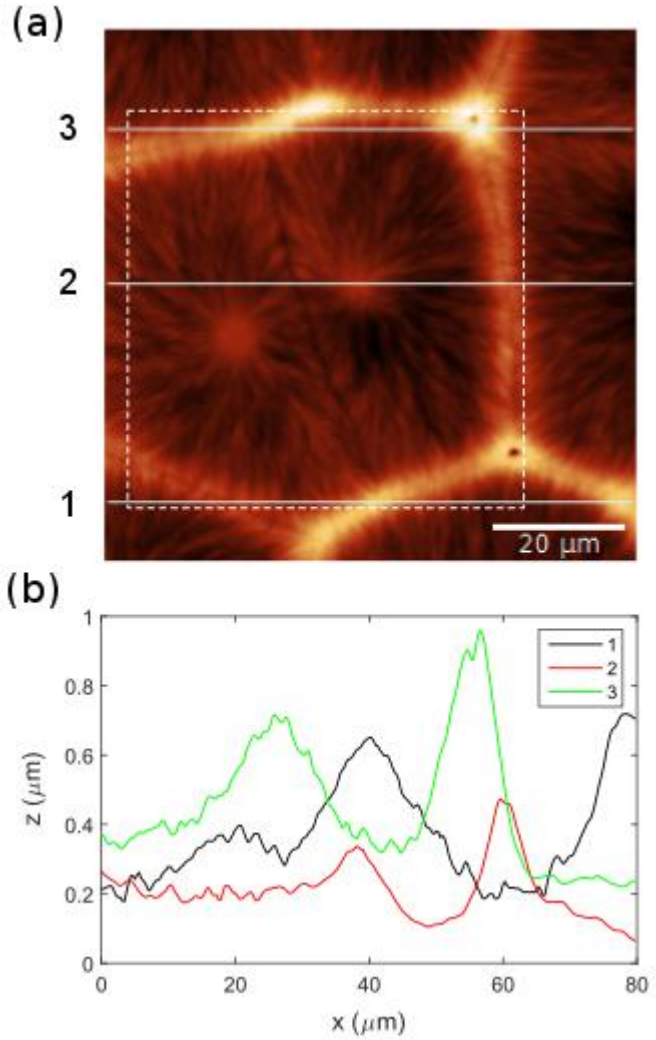

Figure 7 Contact mode AFM topography image (a) and height profile (b) using a conventional AFM from the same surface of crystallized PHB polymer. Black to white colour represents 0 to 1.1 µm in (a). The image was taken after the polymer was fully crystallized. The image size is 80 x 80 μm^2, and the smaller frame in white represents the scan area (57 x 62 μm^2) of the high-speed images shown in figure 7. The image resolution is 256 x 256 pixels. The height profiles from the three white horizontal lines (1-3) are plotted in the bottom graph.

4. Conclusions

The wide applicability of AFM is hindered by the relatively slow imaging rate and, for process control applications in particular, by the low image rate at large scan area. Here we have shown that through the use of a resonating scanner, specifically designed for imaging with large amplitudes, it is possible to scan macroscopic areas with high speed. We have presented a simple but robust quartz bar resonator as the fast scanner. We have demonstrated that scan areas of 170 x 170 μm^2 can be captured in one second, more than four times larger than previous scan areas obtained at comparable frame rates. Although utilizing a quasi-constant height imaging mode, the tip sample-forces remain sufficiently low that it is possible to image a soft, crystallizing polymer without interfering with the process.

Supporting Information for Supplementary Movies and Images

SI1: High-speed images of the same area of a PDMS replica at different time points and scan sizes.

SI2: High-speed movie of crystallizing PHB. Output frame rate increased to 10 frames/sec.

References

[1] Barrett RC and Quate CF 1991 High-speed, large-scale imaging using atomic force microscope *J. Vac. Sci. Technol.* B **9** 302

[2] Schitter G, Allgower F and Stemmer A 2004 A new control strategy for high-speed atomic force microscopy *Nanotechnology* **15** 108-114

[3] Schitter G and Stemmer A 2004 Identification and open-loop tracking control of a piezoelectric tube scanner for high-speed scanning-probe microscopy *IEEE Trans. Contrl. System. Technol.* **12** 449-454

[4] Schitter G, Astrom K J, DeMartini B, Fantner G E, Turner K, Thurner P J and Hansma P K 2006 Design and modelling of a high-speed scanner for atomic force microscopy *Proc. American Control Conference 2006 USA* **WeA15.1** 502-507

[5] Schitter G, Astrom K J, DeMartini B E, Thurner P J, Turner K L, and Hansma P K 2007 Design and Modeling of a High-Speed AFM-Scanner *IEEE Transactions on Control Systems Technology* **15** 906-915

[6] Schitter G, Thurner P J, and Hansma P K 2008 Design and input-shaping control of a novel scanner for high-speed atomic force microscopy *Mechatronics* **18** 282-288

[7] Kodera N, Sakashita M, Ando T 2006 Dynamic proportional-integral-differential controller for high-speed atomic force microscopy *Rev. Sci. Instrum.* **77** 083704

[8] Bozchalooi I Sm Youcef-Toumi K, Burns D J and Fantner G E 2011 Compensator design for improved counterbalancing in high speed atomic force microscopy *Rev. Sci. Instr.* **82** 113712

[9] Yong Y K, Bhikkaji B, and Moheimani S O R 2013 Design, Modeling, and FPAA-Based Control of a High-Speed Atomic Force Microscope Nanopositioner *IEEE/ASME Trans. Mechatronics.* **18** 1060

[10] Walters D A, Cleveland J O, Thomson N H, Hansma P K, Wendman M A, Gurley G and Elings V 1996 Short cantilevers for atomic force microscopy *Rev. Sci. Instrum.* **67** 3583

[11] Sulchek T, Hsieh R, Adams J D, Minne S C, and Quate C F 2000 High-speed atomic force microscopy in liquid *Rev. Sci. Instrum.* **71** 2097

[12] Minne S C, Manalis S R, Quate C F 1995 Parallel atomic force microscopy using cantilevers with integrated piezoresistive sensors and integrated piezoelectric actuators *Appl. Phys. Lett.* **67** 3918

[13] Kitazawa M, Shiotani K, Toda A 2003 Batch fabrication of sharpened silicon nitride tips *Jpn. J. Appl. Phys.* **42** 4844-4847

[14] Viani M B, Schäffer T E, Paloczi G T, Pietrasanta L I, Smith B L, Thompson J B, Richter M, Rief M, Gaub H E, Plaxco K W, Cleland N, Hansma H G, Hansma P K 1999 Fast imaging and fast force spectroscopy of single biopolymers with a new atomic force microscope designed for small cantilevers *Rev. Sci. Instrum.* **70** 4300

[15] Manalis S R, Minne S C and Quate C F 1996 High-speed atomic force microscopy using an integrated actuator and optical lever detection *Appl. Phys. Lett.* **68** 871

[16] Schäffer T and Hansma P K 1998 Characterization and optimization of the detection sensitivity of an atomic force microscope for small cantilevers *J. Appl. Physics* **84** 4661

[17] Ando T, Kodera N, Takai E, Maruyama D, Saito K, and Toda A 2001 A high-speed atomic force microscope for studying biological macromolecules *Proc. Natl. Acad. Sci. USA* **98** 12468

[18] Fantner G, Hegarty P, Kindt J H, Schitter G, Cidade G A G and Hansma P 2005 Data acquisition system for high speed atomic force microscopy *Rev. Sci. Instr.* **76** 026118

[19] Ando T, Kodera N, Maruyama D, Takai E, Saito K, Toda A 2002 A high-speed atomic force microscope for studying biological macromolecules in action *Jpn. J. Appl. Phys.* **41** 4851–4856

[20] Ando T, Uchihashi T, Kodera N, Miyagi A, Nakakita R, Yamashita H, Matada K 2005 High-speed AFM for studying the dynamic behavior of protein molecules at work *J. Surf. Sci. Nanotechnol.* **3** 384-392

[21] Ando T, Uchihashi T, Kodera N, Miyagi A, Nakakita R, Yamashita H, Sakashita M 2006 High-speed atomic force microscopy for studying the dynamic behaviour of protein molecules at work *Jpn. J. Appl. Phys.* **45** 1897–1903

[22] Ando T, Uchihashi T and Fukuma T 2008 High-speed atomic force microscopy for nano-visualization of dynamic biomolecular processes *Progr. Surf. Sci.* **83** 337

[23] Kodera N, Yamamoto D, Ishikawa R, Ando T 2010 Video imaging of walking myosin V by high-speed atomic force microscopy *Nature* **468** 72-76

[24] Shibata M, Yamashita H, Uchihashi T, Kandori H, Ando T 2010 High-speed atomic force microscopy shows dynamic molecular processes in photo-activated bacteriorhodopsin *Nat. Nanotechnol.* **5** 208-212

[25] Vicary J A and Miles M J 2009 Real-time nanofabrication with high-speed atomic force microscopy *Nanotechnol.* **20** 095302

[26] Schitter G and Rost M J 2008 Scanning probe microscopy at video-rate *Materials Today* **11** 40-48

[27] Rost M J, van Baarle G J C, Katan A J, van Spengen W M, Schakel P, van Loo W A, Oosterkamp T H, and Frenken J W M 2009 Video-rate scanning probe control challenges: setting the stage for a microscopy revolution *Asian J. Control* **11** 110-129

[28] Casuso I, Kodera N, Le Grimellec C, Ando T and Scheuring S 2009 Contact-mode high-resolution high-speed atomic force microscopy moview of the purple membrane *Biophys J.* **97(5)** 1354-1361

[29] Fukuma T, Okazaki Y, Kodera N, Uchihashi T, Ando T 2008 High resonance frequency force microscope scanner using inertia balance support *Appl. Phys. Lett.* **92** 243119

[30] Kodera N, Yamashita H, Ando T 2005 Active damping of the scanner for high-speed atomic force microscopy *Rev. Sci. Instrum.* **76** 053708

[31] Yong Y K, Aphale S, and Moheimani S O R 2009 Design, identification and control of a flexure-based XY stage for fast nanoscale positioning *IEEE Trans. Nanotechnol.* **8** 46–54

[32] Braunsmann C and Schäffer T 2010 High-speed atomic force microscopy for large scan sizes using small cantilevers *Nanotechnology* **21** 225705

[33] Watanabe H, Uchihashi T, Kobashi T, Shibata M, Nishiyama J, Yasuda R, and Ando T 2013 Wide-area scanner for high-speed atomic force microscopy *Rev. Sci. Instrum.* **84** 053702

[34] Li J, Deng A, Chen D, Ao Z, Sun Q, Feng J, Yin B, Han L and Han D 2013 High-speed AFM for scanning the architecture of living cells *Nanoscale* **5** 8355

[35] Schitter G and Stemmer A 2003 Model-based signal conditioning for high-speed atomic and friction force microscopy *Microeletronic Enginneering* **67-68** 938-944

[36] Schitter G, Allgower F and Stemmer A 2003 A new control strategy for high-speed atomic force

microscopy *Nanotechnology* **15** 108-114

[37] Schitter G, Stark R W and Stemmer A 2003 Fast contact-mode atomic force microsopcy on biological speciment by model-based control *Ultramicroscopy* **100** 253-257

[38] Schitter G, Stemmer A and Allgower F 2004 Robust two-degree-of-freedom control of an atomic force microscope *Asian J. Contr.* **6** 156-163

[39] Huang P and Andersson S B 2013 High speed atomic force microscopy enabled by a sample profile estimator *Appl. Phys. Lett.* **102** 213118

[40] Tuma T, Lygeros J, Kartik V, Sebastian A and Pantazi A 2012 High-speed multiresolution scanning probe microscopy based on Lissajous scan trajectories *Nanotechnology* **23** 185501

[41] Yong Y K, Moheimani S O R, Petersen I R 2010 High-speed cycloid-scan atomic force microscopy *Nanotechnology* **21** 365503

[42] Mahmood I A and Moheimani S O R 2009 Fast spiral-scan atomic force microscopy *Nanotechnology* **20** 365503

[43] A Ulcˇinas and Š Vaitekonis 2017 Rotational scanning atomic force microscopy *Nanotechnology* **28** 10LT02

[44] Zhao B, Howard-Knight J P, Humphris A D L, Kailas L, Ratcliffe E C, Foster S J, and Hobbs J K 2009 Large scan area high-speed atomic force microscopy using a resonant scanner *Rev. Sci. Instrum.* **80** 093707

[45] Hobbs J K, Vasilev C, Humphris A D L 2006 VideoAFM- a new tool for high speed surface analysis *Analyst* **131** 251-256

[46] Humphris A D L, Miles M J, and Hobbs J K 2005 A mechanical microscope: high-speed atomic force microscopy *Appl. Phys. Lett.* **86** 034106

[47] Hobbs J K, Vasilev C, and Humphris A D L 2005 Real time observation of crystallization in polyethylene oxide video rate atomic force microscopy *Polymer* **46** 10226-10236

[48] Howard-Knight J P and Hobbs J K 2008 Video rate atomic force microscopy using low stiffness, low resonant frequency cantilevers *Appl. Phys. Lett.* **93** 104101

[49] Howard-Knight and Hobbs J K 2011 Finite element modelling of atomic force microscopy cantilever dynamics during video rate imaging *J. Appl. Phys.* **109** 074309

[50] Humphris A D L, Zhao B, Catto D, Howard-Knight J P, Kohli P, and Hobbs J K 2011 High-speed nano-metrology *Rev. Sci. Instrum.* **82** 043710

[51] Seo Y, Choi C S, Han S H, and Han S-J 2008 Real-time atomic force microscopy using mechanical resonator type scanner *Rev. Sci. Instrum.* **79** 103703

[52] Cai W, Zhao J, Gong W, Fan H, and Shang G 2014 Resonance-type bimorph-based high-speed atomic force microscopy: real-time imaging and distortion correction *Meas. Sci. Technol.* **25** 125404

[53] S Timoshenko and J Goodier *Theory of elasticity* McGraw-Hill Inc., US, 3rd Edition, 1970

[54] Hobbs J K and Barham P J 1997 The effect of water on the crystallization of thin films of poly(hydroxybutyrate) *Polymer* **38** 3879-3883

[55] Farrance O E, Jones R A L and Hobbs J K 2009 The observation of rapid surface growth during the crystallization of polyhydroxybutyrate *Polymer* **50** 3730-3938